Int. J. Electrochem. Sci., 10 **(2015)** 3885 - 3896

International Journal of
ELECTROCHEMICAL
SCIENCE
www.electrochemsci.org

Electrochemical Properties of $LiMn_2O_4$ Prepared by Solid-State Combustion Synthesis Using Oxalic Acid as a Fuel

Cancan Peng[1,2], *Hongli Bai*[1,2], *Qiling Li*[1,2], *Yujiao Guo*[1,2], *Jijun Huang*[1,2], *Changwei Su*[1,2], *Junming Guo*[1,2,*]

[1] Key Laboratory of Comprehensive Utilization of Mineral Resources in Ethnic Regions, Yunnan Minzu University, Kunming 650500, PR China
[2] Key Laboratory of Chemistry in Ethnic Medicinal Resources, State Ethnic Affairs Commission & Ministry of Education, School of Chemistry and Biotechnology, Yunnan Minzu University, Kunming 650500, PR China
[*]E-mail: guojunming@tsinghua.org.cn

Received: 6 January 2015 / *Accepted:* 19 February 2015 / *Published:* 23 March 2015

Spinel $LiMn_2O_4$ of the *Fd3m* space group was prepared via solid-state combustion synthesis using oxalic acid as a fuel. Its phase structure and microstructure were characterized by X-ray diffraction (XRD), Fourier transform infrared (FT-IR) spectroscopy and scanning electron microscopy (SEM). The electrochemical performance of material was investigated by galvanostatic charge/discharge, cyclic voltammetry (CV) and electrochemical impedance spectra (EIS). The XRD patterns indicate that samples containing oxalic acid are single-crystalline phase of $LiMn_2O_4$. SEM images show that samples containing oxalic acid are composed of spherical-like particles whereas the sample without oxalic acid is composed of agglomerated clusters. At 0.2 C, galvanostatic charge/discharge experiments demonstrate that the discharge capacity of samples increases with an increase in oxalic acid content up to 5 wt% and it decreases at an oxalic acid content of ≥10 wt%. The specimen containing 5 wt% oxalic acid possesses the highest initial discharge capacity. CV and EIS results further confirm that this sample has the best electrochemical activity.

Keywords: Oxalic acid; Solid-state combustion synthesis; Spinel $LiMn_2O_4$; Lithium-ion battery

1. INTRODUCTION

The lithium-ion battery (LIB), as a medium of electrochemical energy storage and conversion, was first commercialized by Sony in 1991 and owes its name to the exchange of Li^+ ions between a graphite anode and a layered-oxide cathode [1]. It is regarded as a promising new power source for hybrid electric vehicles because of its long cycle life, elevated energy density, high working voltage and low self-discharge rate compared with other rechargeable systems [2]. Since the

commercialization of lithium-ion secondary batteries, they occupy a prime position in the commercial market for powering portable electronic devices such as laptops, personal digital assistants, and cellular phones. They have been listed as candidates for aerospace power supplies, military and energy storage. The traditional cathode materials mainly include layered $LiCoO_2$, olivine $LiFePO_4$ and spinel $LiMn_2O_4$ [3]. However, spinel $LiMn_2O_4$ has received much attention as one of the most competitive positive-electrode materials for LIBs due to its abundant resources, low cost, high safety and environmental friendliness [4].

It is well documented that the electrochemical performance of cathode materials effectively depends on their physical and chemical properties including structural integrity, crystallite size, phase homogeneity and microstructure [5,6]. Furthermore, most of these physicochemical parameters are influenced by the synthetic process used [7,8]. Conventional methods for the preparation of $LiMn_2O_4$ contains solid-state reaction [9], co-precipitation [10], sol-gel method [11], hydrothermal synthesis [12] Pechini method [13], etc. The traditional solid-state synthesis process can achieve the industrial-scale production of spinel $LiMn_2O_4$ with convenient operation but it suffers from the long-range diffusion of metal ions, which may result in inhomogeneity, a larger particle size and longer calcination times [14]. Our research group has investigated the influence of various fuels on solid-state combustion synthesis. These fuels include glucose [6] and citric acid [15]. Experimental results show that different fuels can greatly affect the particle morphology and electrochemical performance of the products. The micro-morphology of samples prepared using an acid fuel is mainly a spherical-like particle while the micro-morphology of specimens prepared using glucose is a lump. In this research, spinel $LiMn_2O_4$ with *Fd3m* space group was rapidly prepared by solid-state combustion synthesis using oxalic acid as the fuel. The crystalline structure, micro-morphology and electrochemical performance of the products were investigated in detail. Compared with glucose and citric acid, oxalic acid gives more uniform particle sizes and a narrower size distribution range (0.10-1.5 μm).

2. EXPERIMENTAL

2.1 Material preparation

Lithium carbonate (AR, Sinopharm) and manganese carbonate (AR, Tianjin Kemiou) were used as metal source materials and oxalic acid (AR, Tianjin No. 3 Chemical Reagent Factory) was used as the fuel. Lithium carbonate and manganese carbonate were weighed to give a stoichiometric ratio of Mn:Li = 2:1, and then the metal carbonates were placed in a 500 mL polytetrafluoroethylene jar with an ethanol medium. A specific amount of oxalic acid was then added to the mixture and the raw materials together with oxalic acid were ball-milled thoroughly by planetary ball mill. After evaporation of the solvent, the mixture was ground into white powder until a flour-like consistency was obtained. About 5 g of the powder was combusted in a muffle furnace at 500 °C for 1 h. Ultimately, the alumina crucible containing the starting materials was removed and the target $LiMn_2O_4$ product was obtained after the starting materials spontaneously cooled to ambient temperature. To

determine the impact of the amount of oxalic acid on the electrochemical properties of $LiMn_2O_4$, a mass percentage series of 0 wt%, 5 wt%, 10 wt%, 20 wt% and 30 wt% were prepared.

2.2 Sample characterization

Differential thermal analysis (DTA) and thermogravimetry (TG) measurements were carried out in an air atmosphere using a TG-DSC thermal analyzer system (STA449F3, NETZSCH) at a heating rate of 10 °C/min from 40 to 700 °C. Fourier transform infrared (FT-IR) spectroscopy of the as-prepared material was conducted using KBr pellets in the 400 to 800 cm^{-1} range with a Nicolet IS10 spectrometer. Powder X-ray diffraction (XRD, D/max-TTRIII, Japan) with Cu Kα radiation was used to identify the crystalline phase of the prepared powders. XRD data were collected at 2θ = 10-70° with a step width of 0.02°, a scan speed of 4°/min, an operating current of 30 mA and a voltage of 40 kV. The morphologies of the as-prepared powders were determined by scanning electron microscopy (SEM, QUANTA 200, America FEI).

2.3 Cell assembly and electrochemical evaluation

Electrochemical performance was evaluated using CR2025 coin-type cells assembled in a glove box (MBraun, Germany) filled with high-purity argon gas. The positive electrodes were prepared by homogeneously coating a syrupy N-methyl-pyrrolidone (NMP) solution composed of 80 wt% active material, 10 wt% acetylene black, and 10 wt% polyvinylidene fluoride (PVDF) onto clean and polished aluminum foil by the doctor-blade technique. It was then cut into small disks 16 mm in diameter under a specific pressure, and before assembling the cells these small disks were dried at 120 °C under vacuum for 12 h. Lithium metal foil, 1 M $LiPF_6$ dissolved in ethylene carbonate (EC)-diethyl carbonate (DEC) (1:1, v/v) and a Celgard 2320-type membrane were used as the counter electrode, the electrolyte and a microporous polypropylene separator, respectively.

At room temperature, charge-discharge experiments were carried out galvanostatically using a cut-off voltage limit of 3.20-4.35 V (versus Li/Li^+) at 0.2 C with a Land electric test system CT2001A (Wuhan Jinnuo Electronic Co., Ltd). Cyclic voltammogram (CV) measurements were obtained at room temperature on a ZAHNER Zennium IM6 Electrochemical Workstation (ZAHNER-elektrik GmbH & Co. KG, Kronach, Germany) at a scan rate of 0.2 mV/s over a voltage range of 3.6 V to 4.5 V (versus Li/Li^+). Electrochemical impedance spectroscopy (EIS) measurements of the cells were obtained using an IM6ex electrochemical workstation. The frequency ranged from 0.1 Hz to 100 KHz with an applied AC signal amplitude of 10 mV.

3. RESULTS AND DISCUSSION

3.1 Thermal analysis of the precursor

Fig. 1 shows TG-DSC curves of the $LiMn_2O_4$ obtained from the precursor containing 5 wt% oxalic acid. The weight loss of the precursor can be roughly divided into four parts in the 40-700 °C

range. The minor weight decrease before 340 °C comes from the volatilization of water adsorbed on the sample surface.

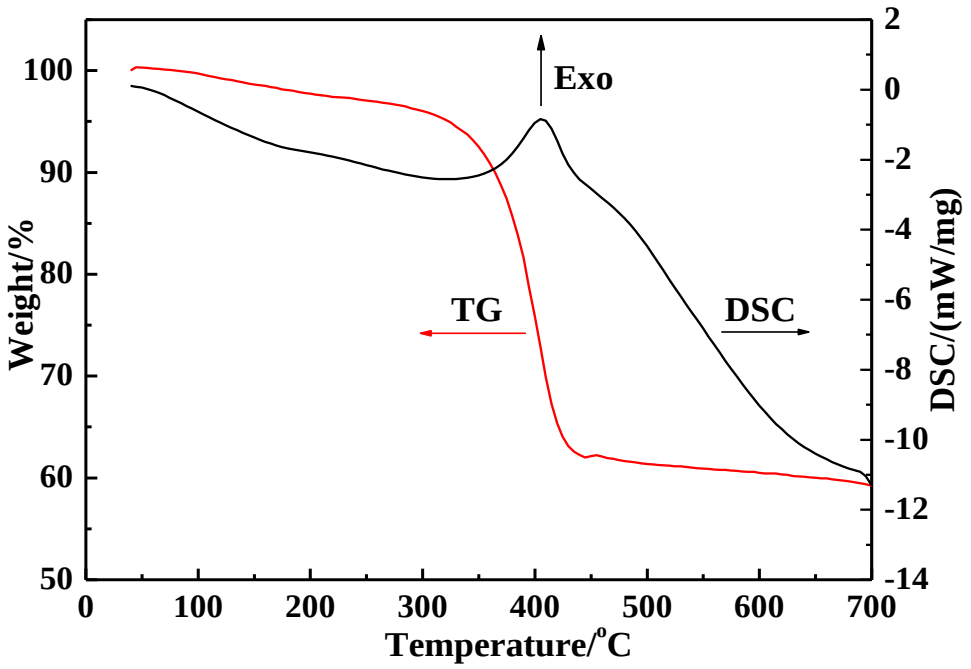

Figure 1. TG-DSC curves of $LiMn_2O_4$ obtained from the precursor with 5 wt% oxalic acid.

The significant weight loss accompanied by an acute exothermic peak around 340-400 °C corresponds to the decomposition reactions of metal carbonate and fuel. In this stage, a considerable amount of carbon dioxide is continously released which contributes to the major total weight loss. From 400 °C to 500 °C, just a small amount of weight loss can be observed in the TG curves. At higher than 500 °C, the TG curve is almost flat with negligible weight loss, implying the formation of a stable spinel complex oxide at 500 °C [16].

3.2 Crystal phase and microstructural characterization

Fig. 2 compares the FT-IR spectra of the as-prepared powders in a wavelength range of 400-800 cm^{-1} and these were recorded at room temperature. Two characteristic absorption bands from the Mn(IV)-O and Mn(III)-O asymmetrical stretching vibration of the MnO_6 octahedron are present at 615 cm^{-1} and 510 cm^{-1}, respectively [17].

A typical XRD pattern of each sample is shown in Fig. 3. The well-defined reflection peaks include eight lattice planes at (111), (311), (222), (400), (331), (511) (440) and (531). These are all indexed to the cubic structure of spinel $LiMn_2O_4$ (JCPDS File No. 35-0782) with a *Fd3m* space group. The sample without oxalic acid contained trace amounts of the Mn_2O_3 phase, but no peaks for impurity phase were detected in the samples containing oxalic acid. Results show that adding moderate amount of oxalic acid as a fuel could improve the purity of products.

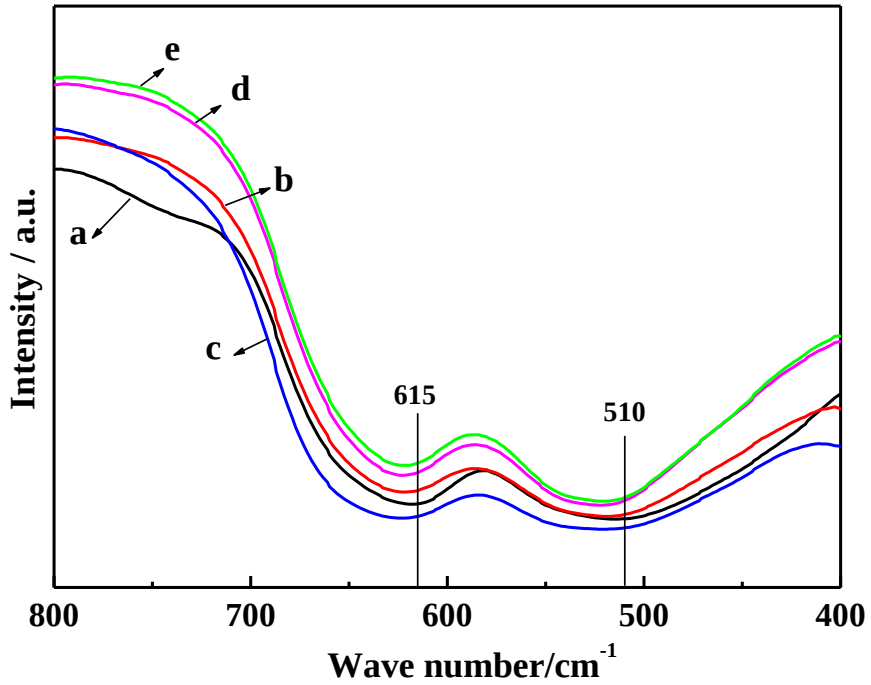

Figure 2. FT-IR spectra of $LiMn_2O_4$ with (a) 0 wt%, (b) 5 wt%, (c) 10 wt%, (d) 20 wt% and (e) 30 wt% oxalic acid, respectively.

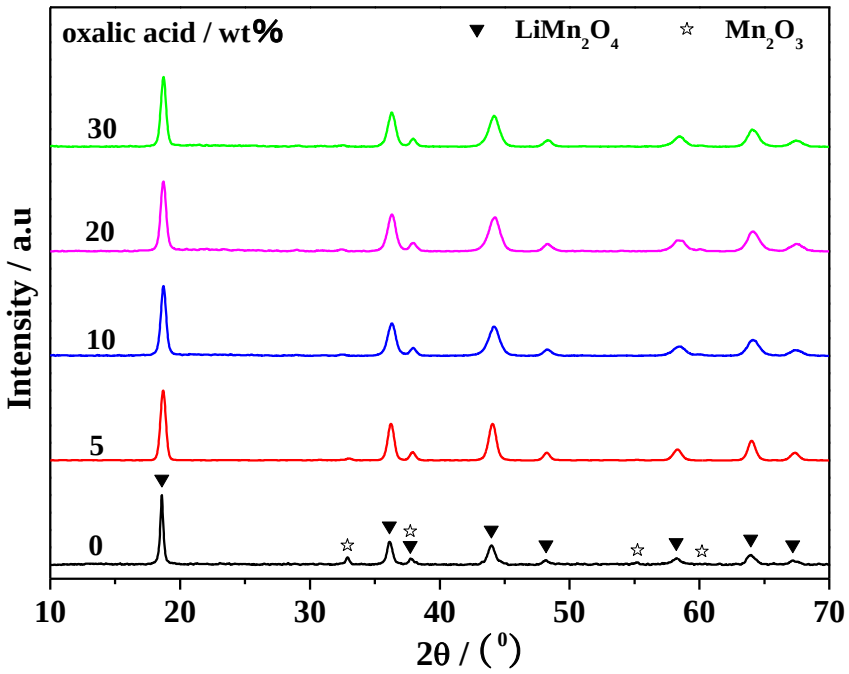

Figure 3. XRD patterns of $LiMn_2O_4$ prepared with different amount of oxalic acid.

SEM images of the $LiMn_2O_4$ powder after the combustion reaction are shown in Fig. 4. It is evident that the particle size and granularity distribution of the $LiMn_2O_4$ material showed distinct changes after the addition of oxalic acid. The sample prepared without oxalic acid agglomerated in clusters; however, the samples obtained with the addition of oxalic acid are spherical-like particles

with homogeneous granularity, a clear surface boundary and a narrow size distribution of 0.10-1.5 μm. The morphology of samples obtained with the addition of oxalic acid is basically identical to that of the product obtained with the addition of citric acid as a fuel [15]. Apparently, with an increase in the amount of oxalic acid, the agglomeration of the powders is limited, leading to smaller particles, a clearer interface and larger interspaces.

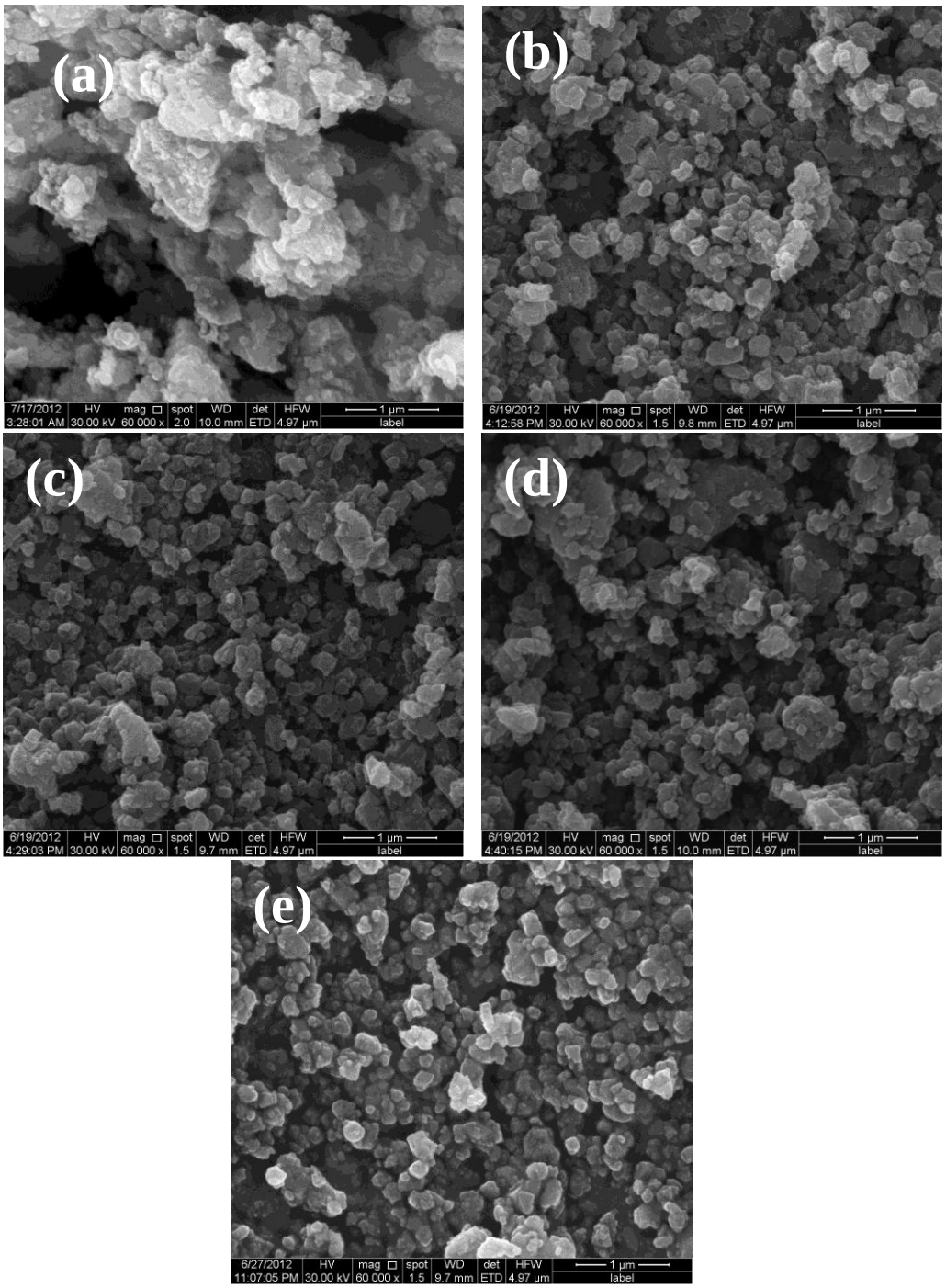

Figure 4. SEM images of $LiMn_2O_4$ with (a) 0 wt%, (b) 5 wt%, (c) 10 wt%, (d) 20 wt% and (e) 30 wt% oxalic acid, respectively.

A large interspace between particles is advantageous for electrolyte permeation into cathode materials and for the intercalation-deintercalation of lithium ions during the charge-discharge process. Therefore, it may improve the electrochemical performance of the $LiMn_2O_4$ cathode material.

3.3 Electrochemical performance

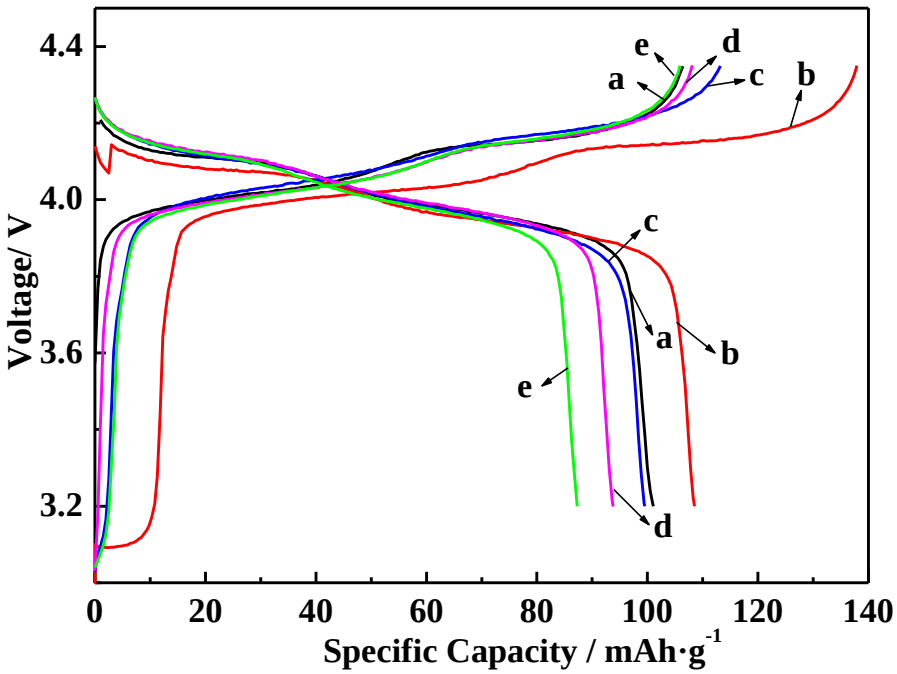

Figure 5. The initial galvanostatic charge-discharge curves of $LiMn_2O_4$ products with (a) 0 wt%, (b) 5 wt%, (c) 10 wt%, (d) 20 wt% and (e) 30 wt% oxalic acid, respectively.

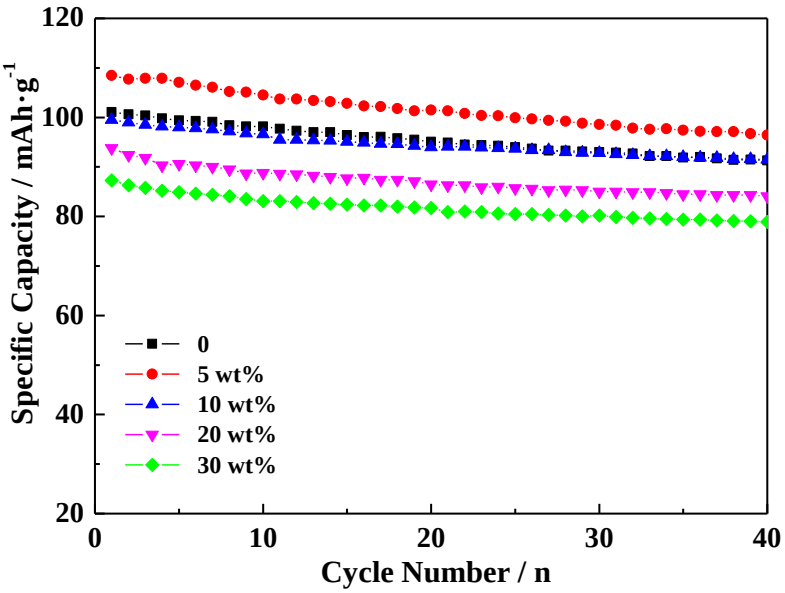

Figure 6. Cycling performance of the $LiMn_2O_4$ electrodes synthesized with various amount of oxalic acid.

Fig. 5 and Fig. 6 show the initial galvanostatic charge-discharge profiles and the cycling performance curves of the products, respectively. The voltage range was 3.20-4.35 V (vs. Li/Li^+) at 0.2 C and at room temperature. All the samples gave two well-defined voltage plateaus during the charge-discharge process and these coincide with Li^+ insertion and extraction at two different tetragonal 8a sites in the spinel framework [18].

Table 1. The discharge specific capacity and capacity retention of $LiMn_2O_4$ after 40 cycles.

Oxalic acid amount (wt%)	Discharge specific capacity (mAh/g)		Capacity retention (%)
	First cycle	40^{th} cycle	
0	101.5	90.40	89.06
5	108.5	96.70	89.12
10	99.50	91.00	91.46
20	93.80	84.40	89.98
30	87.30	79.30	90.84

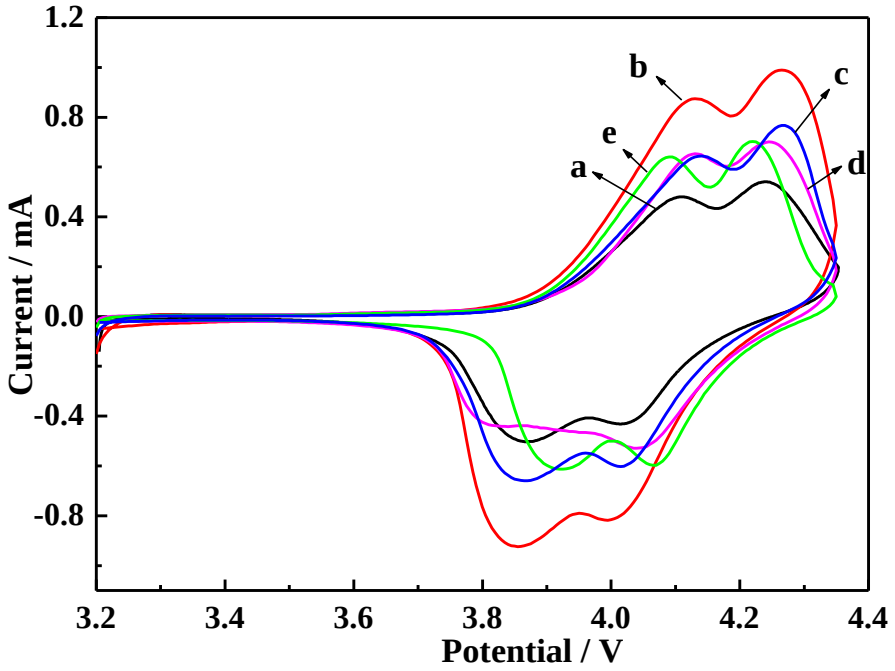

Figure 7. Cyclic voltammogram of the 10^{th} cycle of cathode materials with (a) 0 wt%, (b) 5 wt%, (c) 10 wt%, (d) 20 wt% and (e) 30 wt% oxalic acid, respectively.

Table 1 lists the discharge specific capacity and the capacity retention after 40 cycles for the cathode materials. Clearly, with an increase in the amount of oxalic acid from 0 wt% to 30 wt%, the

initial discharge capacity of the products increases gradually to a maximum value of 108.5 mAh/g for the 5 wt% product and then decreases with an increase in the amount of oxalic acid from 10 wt% to 30 wt%. After the 40th cycle, the 10 wt% oxalic acid specimen gave the highest capacity retention of 91.46%, and its capacity retention only increased by 2.40% compared with the sample without oxalic acid.

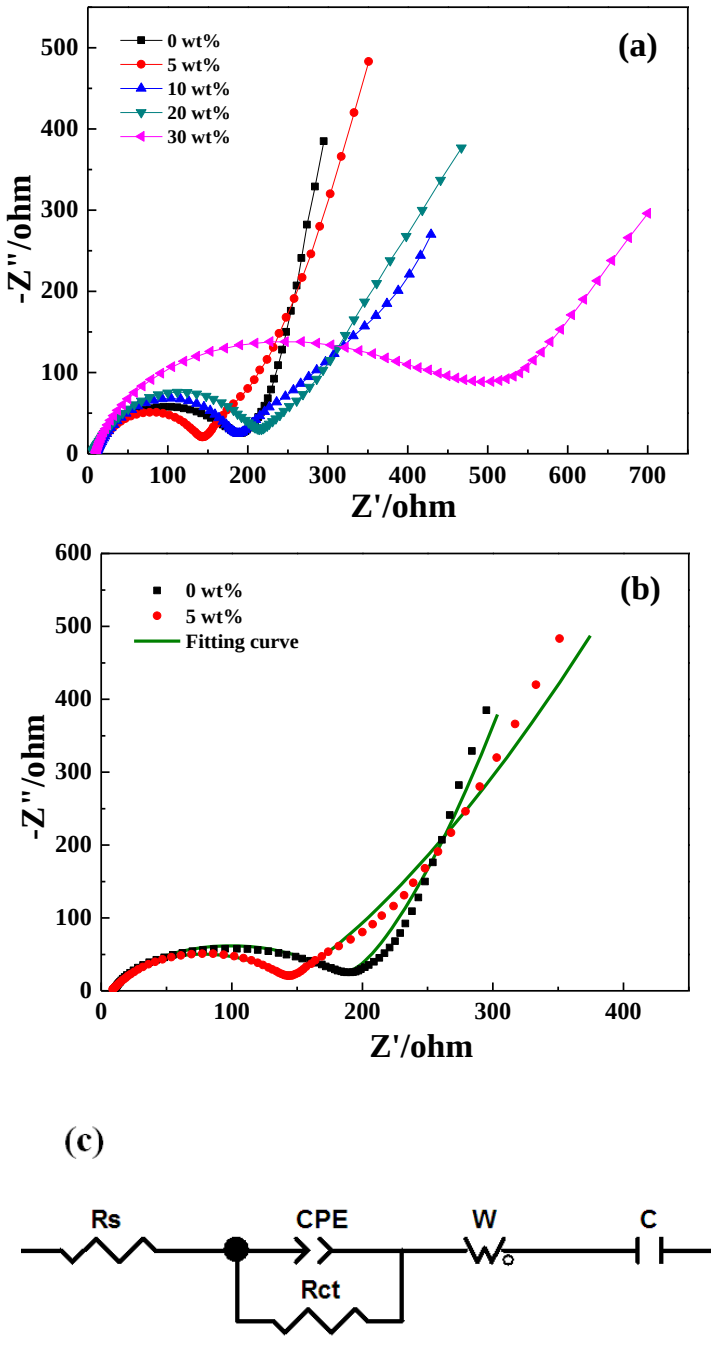

Figure 8. (a) The electrochemical impedance spectra of all cathode materials after 10 charge-discharge cycles, (b) EIS plots of $LiMn_2O_4$ electrodes with 0 wt% and 5 wt% oxalic acid and (c) The corresponding equivalent circuit simulated by ZView software.

Thus, adding oxalic acid as a fuel does not greatly influence the cycling performance of the products.

Cyclic voltammograms (CV) of all the samples after the 10^{th} cycle are shown in Fig. 7. Two pairs of redox peaks were presented in the CV curves and this is consistent with the two distinct plateaus in the charge-discharge curves of Fig. 5. Moreover, the CV curve of the product containing 5 wt% oxalic acid is characterized by two highly distinct oxidation current peaks at high potential, two highly distinct reduction current peaks at low potential and a relatively large integrated area. This indicates the cathode material has better electrochemical activity and a reversible oxidation reaction process [19].

Fig. 8 (a) shows the electrochemical impedance spectra of all the cathode materials after 10 charge-discharge cycles. EIS plots of the $LiMn_2O_4$ electrodes containing 0 wt% and 5 wt% oxalic acid are shown in Fig. 8 (b) while Fig. 8 (c) is the corresponding equivalent circuit. The parameters of the impedance spectra in Fig. 8 (b) were simulated using ZSimpWin. Table 2 lists the fitting results.

The impedance spectra of $LiMn_2O_4$ are characterized by an oblate semicircle in the middle-frequency region and a sloping line in the low-frequency range. An intercept at the Z_{real} axis in the high-frequency region corresponds to the ohmic resistance (R_s) of the electrolyte. The depressed semicircle in the middle-frequency range is related to the charge transfer resistance (R_{ct}). The sloped line in the low-frequency range represents the Warburg impedance (W) that corresponds to the lithium-ion diffusion process.

Table 2. The fitting values of electrochemical parameters obtained from EIS.

Parameter (Ω)	Oxalic acid amount (wt%)	
	0	5
R_s	8.963	6.429
R_{ct}	173.4	119

From Fig. 8 (a), with an increase in the amount of oxalic acid, the R_{ct} value first decreases to a minimum and then gradually increases. Combined with the data from Table 2, the R_{ct} reaches a minimum of 119 Ω for the 5 wt% oxalic acid product, which is far lower than that of the sample without oxalic acid (173.4 Ω). This fact further confirms that adding a moderate amount of oxalic acid can improve the electronic conductivity of the $LiMn_2O_4$ electrode and enhance the electrochemical performance of the cathode material [19-21].

4. CONCLUSIONS

Oxalic acid was used as an assistant fuel to synthesize spinel type $LiMn_2O_4$ by a simple and efficient solid-state combustion synthesis at 500 °C for 1 h. The influence of the amount of fuel on the physicochemical properties of the products is discussed in detail. XRD patterns reveal that the main phase of the material is spinel $LiMn_2O_4$. SEM images indicate that the as-synthesized $LiMn_2O_4$ without oxalic acid consists of agglomerated clusters; however, the products obtained upon the addition of oxalic acid are uniformly distributed spherical-like particles with a clear surface boundary and a slightly reduced particle size. Electrochemical results show that the $LiMn_2O_4$ electrode containing 5 wt% oxalic acid exhibits the highest initial discharge capacity of 108.5 mAh/g. Both the CV and EIS tests also indicate that the specimen containing 5 wt% oxalic acid possesses superior electrochemical reversibility and optimal electrochemical activity.

ACKNOWLEDGEMENTS
This work was financially supported by the National Natural Science Foundation of China (51262031, 51462036), Program for Innovative Research Team (in Science and Technology) in University of Yunnan Province (2010UY08, 2011UY09), Yunnan Provincial Innovation Team (2011HC008), the Natural Science Foundation of Yunnan Provincial Education Department (2014J079), and Innovation Program of Yunnan Minzu University (2013HXSRTY01, 2014YJZ10, 2014YJY74).

References

1. M. Armand and J.-M. Tarascon, *Nature.* 451 (2008) 652-657.
2. Jingwen Yao, Feng Wu, Xinping Qiu, Ning Li and Yuefeng Su, *Electrochim Acta*. 56 (2011) 5587-5592.
3. Mingwu Xiang, Chang-Wei Su, Lili Feng, Minglong Yuan and Junming Guo, *Electrochim Acta*. 125 (2014) 524-529.
4. Tian Qiu, Juan Wang, Yanluo Lu and Wensheng Yang, *Electrochim Acta*. 147 (2014) 626-635.
5. S.J. Shi, J.P. Tu, Y.Y. Tang, Y.X. Yu, Y.Q. Zhang, X.L. Wang and C.D. Gu, *J. Power Sources*. 228 (2013) 14-23.
6. Xianyan Zhou, Mimi Chen, Mingwu Xiang, Hongli Bai and Junming Guo, *Ceram Int*. 39 (2013) 4783-4789.
7. P. Kalyani, N. Kalaiselvi and N.Muniyandi, *J. Power Sources*. 111 (2002) 232-238.
8. A. Subramania, N. Angayarkanni and T. Vasudevan, *Mater Chem Phys*. 102 (2007) 19-23.
9. Xiaoyu Feng, Yun Tian, Jianxin Zhang and Longwei Yin, *Powder Technol*. 253 (2014) 35-40.
10. R. Thirunakaran, R. Ravikumar, S. Gopukumar and A. Sivashanmugam, *J Alloy Compd*. 556 (2013) 266-273.
11. B. Hamankiewicz, M. Michalska, M. Krajewski, D. Ziolkowska, L. Lipinska, K. Korona, M. Kaminska and A. Czerwinski, *Solid State Ionics*. 262 (2014) 9-13.
12. C.H. Jiang, S.X. Dou, H.K. Liu, M. Ichihara and H.S. Zhou, *J. Power Sources*. 172 (2007) 410-415.
13. Yi-Sup Han and Ho-Gi Kim, *J. Power Sources*. 88 (2000) 161-168.
14. Chunyu Zhu, Akira Nobuta, Genki Saito, Isao Nakatsugawa and Tomohiro Akiyama, *Adv Powder Technol.* 25 (2014) 342-347.

15. Xianyan Zhou, Mimi Chen, Hongli Bai, Changwei Su, Lili Feng and Junming Guo, *Vacuum*. 99 (2014) 49-55.
16. Yaqing Weng, Shengming Xu, Guoyong Huang and Changyin Jiang, *J Hazard Mater*. 246-247 (2013) 163-172.
17. Xifei Li, Youlong Xu and Chunlei Wang, *J Alloy Compd*. 479 (2009) 310-313.
18. D. Arumugam, G. Paruthimal Kalaignan, Kumaran Vediappan and Chang Woo Lee, *Electrochim Acta.* 55 (2010) 8439-8444.
19. Hai Ming, Yuerong Yan, Jun Ming, Jason Adkins, Xiaowei Li, Qun Zhou and Junwei Zheng, *Electrochim Acta*. 120 (2014) 390-397.
20. Biao Zhang, Zhen-Dong Huang, Sei Woon Oh and Jang-Kyo Kim, *J. Power Sources*. 196 (2011) 10692-10697.
21. Tingfeng Yi, Longcheng Yin, Yongquan Ma, Haoyu Shen, Yanrong Zhu and Rongsun Zhu, *Ceram Int.* 39 (2013) 4673-4678.